Applied Physics Letters ARTICLE scitation.org/journal/apl

Niobium diselenide superconducting photodetectors

Cite as: Appl. Phys. Lett. **114**, 251103 (2019); doi: 10.1063/1.5097389
Submitted: 25 March 2019 · Accepted: 31 May 2019 ·
Published Online: 27 June 2019

G. J. Orchin,[1,a] D. De Fazio,[2] A. Di Bernardo,[3] M. Hamer,[4] D. Yoon,[2] A. R. Cadore,[2] I. Goykhman,[2] K. Watanabe,[5] T. Taniguchi,[5] J. W. A. Robinson,[3] R. V. Gorbachev,[4] A. C. Ferrari,[2] and R. H. Hadfield[1]

AFFILIATIONS

[1]School of Engineering, University of Glasgow, Glasgow G12 8QQ, United Kingdom
[2]Cambridge Graphene Centre, University of Cambridge, Cambridge CB3 0FA, United Kingdom
[3]Department of Materials Science & Metallurgy, University of Cambridge, Cambridge CB3 0FS, United Kingdom
[4]National Graphene Institute, The University of Manchester, Manchester M13 9PL, United Kingdom
[5]National Institute for Materials Science, 1-1 Namiki, Tsukuba 306-0044, Japan

[a]**Author to whom correspondence should be addressed:** g.orchin.1@research.gla.ac.uk

ABSTRACT

We report the photoresponse of niobium diselenide ($NbSe_2$), a transition metal dichalcogenide which exhibits superconducting properties down to a single layer. Devices are built by using micromechanically cleaved 2–10 layers and tested under current bias using nano-optical mapping in the 350 mK–5 K range, where they are found to be superconducting. The superconducting state can be perturbed by absorption of light, resulting in a voltage signal when the devices are current biased. The response is found to be energy dependent, making the devices useful for applications requiring energy resolution, such as bolometry, spectroscopy, and infrared imaging.

The potential of superconducting materials for low noise photon detection has long been recognized.[1,2] Several concepts exploiting superconductors have further evolved, including transition edge sensors (TESs),[3] kinetic inductance detectors (KIDs),[4] and superconducting nanowire single photon detectors (SNSPDs).[5,6] SNSPDs can be built with >90% single photon detection efficiency at 1550 nm (Ref. 7), and have found applications in quantum optics,[8] quantum key distribution,[9] single photon LIDAR,[10] and infrared astronomy.[1] In SNSPDs, a single photon impinges upon a current-biased superconducting nanowire, generating a local resistive region (hotspot).[11] This makes the superconducting current diverge around it, increasing the current density in the surrounding areas. The devices can be operated under bias conditions, so that the current density in the regions adjacent to the hotspot breaks the superconducting state, causing the formation of a resistive barrier.[12] Current is then forced to cross the barrier, which can be sensed by a readout circuit. The photon wavelength required to trigger an SNSPD is inversely proportional to its width.[13] Thus, decreasing the width reduces the photon energy needed to trigger an SNSPD. However, this requires nanometer-precision in lithographic tools. An alternative approach is to decrease the device thickness, as this will reduce the cross section of the superconducting wire, allowing single photon detection for wider wires.[14]

$NbSe_2$ is a superconductor with a bulk superconducting transition temperature (T_c) ~ 7.2 K.[15] In the layered 2H form, which we use here, one layer (1L) consists of a sheet of Nb atoms sandwiched between two sheets of Se atoms and arranged in a hexagonal structure.[16] Crystals can be exfoliated to produce flakes down to 1L.[16,17] Reference 17 showed that $NbSe_2$ is superconducting down to 1L, with $T_c \sim 2$ K, while 2L-$NbSe_2$ has $T_c \sim 5$ K,[17] above the 4.2 K liquid He temperature used in SNSPD measurement setups.[8] This paves the way for studying few-layer $NbSe_2$ superconducting detectors.

Here, we use micrometer-sized 2–10L $NbSe_2$ flakes as superconducting detectors for 1550 nm pulsed illumination in the 5 K–350 mK range. We find a nonlinear response with a minimum noise equivalent power (NEP) ~32 fW $Hz^{-0.5}$, at a laser pulse energy of 27 fJ. This is comparable with cryogenic graphene hot electron bolometers[18] and commercial InGaAs photodiodes.[19,20]

The detectors are fabricated as follows. We use a substrate with 285 nm SiO_2 on Si, for optimal optical contrast.[21,22] On this, we fabricate Ti/Au (5 nm/50 nm) contacts by evaporation and lift-off. Bulk

$NbSe_2$ is sourced from HQ graphene.[23] Reference 24 showed that $NbSe_2$ can degrade in air due to the reaction of Nb with O_2. Thus, an exfoliated sample left unprotected for several hours would be unlikely to show superconductivity.[17] It is therefore necessary to encapsulate $NbSe_2$ with an impermeable membrane, such as a flake of hexagonal boron nitride (hBN).[17] Here, we use hBN crystals grown by the temperature-gradient method under high pressures and at high temperatures.[25] hBN and $NbSe_2$ flakes are exfoliated by micromechanical cleavage on Nitto Denko tape,[26] then exfoliated again on a polydimethylsiloxane (PDMS) stamp, placed on top of a glass slide, for inspection under an optical microscope. This yields large (up to $\sim 100\,\mu$m) flakes.[27] Few-layer (FL) flakes are selected based on optical contrast and then stamped on the contacts with a micromanipulator. FL-hBN flakes are exfoliated on tape, then on SiO_2/Si for microscope inspection. Thin flakes (up to 10 nm), selected by optical contrast, are picked with a polycarbonate (PC)/PDMS stack prepared on a microscope glass slide.[28] The stack is then mounted on a micromanipulator under an optical microscope and transferred on FL-$NbSe_2$ to protect it from air-exposure. The temperature is increased to $\sim 100\,^{\circ}$C to release PC, which is then dissolved in chloroform.[29] 30 devices of 2–10L-$NbSe_2$ were prepared to check reproducibility and the effect of thickness on device performance. We did not use 1L-$NbSe_2$ due to its T_c being lower than 4.2 K.[17]

Raman spectroscopy in vacuum is performed by mounting an Oxford Instruments vacuum stage under a 50× ultralong working distance objective of a Horiba LabRam Evolution spectrometer. A turbomolecular pump is used to achieve a base pressure of $\sim 10^{-5}$ Torr. Measurements are done with 514 nm excitation, with an 1800 grooves/mm grating and a spectral resolution $\sim 0.3\,\text{cm}^{-1}$. The power is kept below 300 μW to avoid any damage. Figure 1(a) plots the low frequency ($<100\,\text{cm}^{-1}$) spectrum of a $NbSe_2$ flake after hBN encapsulation and that of bulk $NbSe_2$. The shear modes (C) are due to the relative motions of the atomic planes.[30–32] The position of the C peak, Pos(C), can be used to derive the number of layers (N) as[32]

$$N = \frac{\pi}{2\cos^{-1}\left[\frac{\text{Pos(C)}_N}{\text{Pos(C)}_\infty}\right]}, \tag{1}$$

where Pos(C)_∞ is Pos(C) in the bulk. Figure 1(a) gives Pos(C)_∞ $\sim 28.6\,\text{cm}^{-1}$ (red curve) and $\sim 26.2\,\text{cm}^{-1}$ (blue curve). Thus, N ∼ 4.

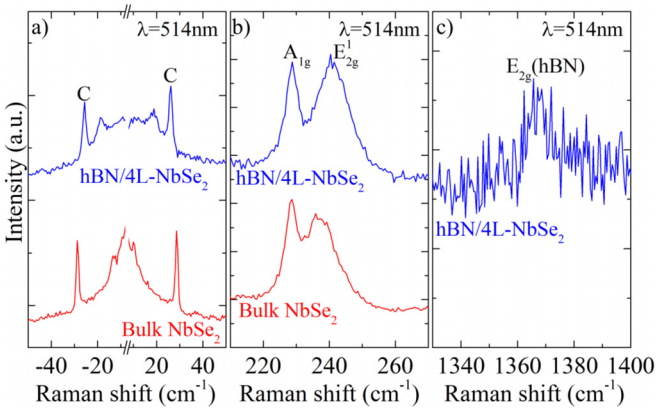

FIG. 1. (a)–(c) Raman spectra of hBN/4L-$NbSe_2$ (blue) and bulk $NbSe_2$ (red).

The hBN E_{2g} peak[33,34] is at $\sim 1367\,\text{cm}^{-1}$ in Fig. 1(c) and it has a full width at half maximum (FWHM) of $\sim 9\,\text{cm}^{-1}$, as expected for ∼10 nm hBN.[35]

Optical measurements are then performed in a closed cycle 2-stage Pulse Tube with an additional ^{3}He stage capable of reaching a base temperature $T_{base} \sim 350$ mK, equipped with a bespoke confocal microscope with piezoelectric positioners.[36] This allows repositioning of the focused laser spot without warming up the sample.

The current necessary to break the superconducting state, the critical current I_c,[37] is measured at T_{base}, Fig. 2(a). I_c is identified by the sudden change in slope in the current biased I-V. The measurement is carried out in a two-wire configuration. A series resistance of 12 Ω arises due to the cryostat wiring and contact resistance with the $NbSe_2$ flake. The I-V curves are increasingly hysteretic as the temperature is decreased [Fig. 2(b)]. The current at which superconductivity is reestablished, the retrapping current, I_r,[38] is as low as half I_c at 360 mK. This is because electrical heating generated in the resistive state cannot be dissipated and increases the sample temperature. We obtain $I_c(0) = 677\,\mu$A and $T_c = 6$ K.

Using a 1 μW continuous wave 1550 nm laser, the confocal microscope is raster scanned over the device using piezoelectric positioners. The resulting reflection is used to construct an image of the device area at 5 K [Fig. 3(b), blue-yellow]. To locate the photosensitive area, the $NbSe_2$ devices are current biased at $0.9I_c$ (227 μA) using the circuit shown in Fig. 4. A programable pulse generator is then used to drive a 1550 nm laser diode at 1 MHz repetition rate with 20 ns pulse width. The laser power is attenuated to ∼17 fJ per pulse (measured at the fiber optic input to the cryostat) and scanned over the device. The resulting voltage signals are amplified with 46 dB gain over the bandwidth 10 kHz–500 MHz using a room temperature low noise amplifier (RF Bay LNA-545), and voltage pulses are counted by a universal counter (Agilent 53132A). As shown in Fig. 3(b) (white-red contour lines), the photosensitive area is centered between the two electrical contacts indicating that the superconducting $NbSe_2$ is the photosensitive element. There also appears to be a nonuniform response across the device area. This is attributed to the nonuniform current density in $NbSe_2$ as a result of contact geometry and partial oxidation.

Using the readout circuit in Fig. 4(a) a 4L-$NbSe_2$ flake is current biased and illuminated with single shot laser pulses. The resulting voltage signals are measured with an oscilloscope (8 GHz Infiniium 80804A), where the voltage observed will be proportional to the resistance of the detector, within the bandwidth of the amplifier

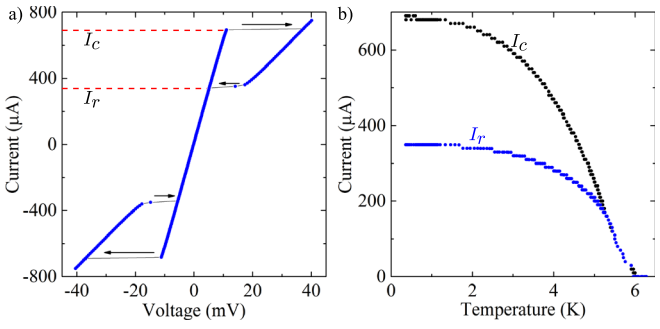

FIG. 2. (a) Current-voltage (I-V) measurements of a 4L-$NbSe_2$ device at 360 mK. (b) Temperature dependence of I_c and I_r.

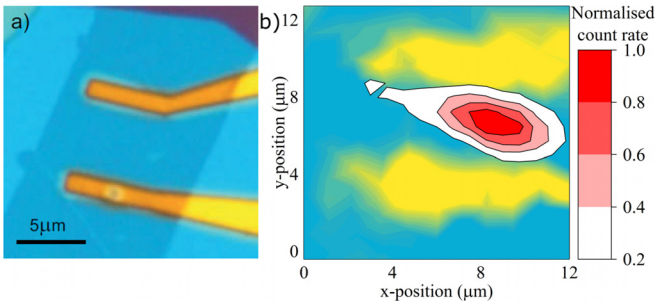

FIG. 3. (a) Optical image of a 4L-$NbSe_2$ flake, covered by ~10 nm hBN (light blue) transferred on Au electrodes. (b) False color image of the same sample at 5 K using 1550 nm illumination with 2.5 μm FWHM. White to red contour lines show the normalized count rate for 17 fJ pulses, thus the optically sensitive area of the detector.

(10 kHz–500 MHz). When the detector is biased between I_c and I_r [Fig. 2(b)], a bright optical pulse results in a latched response, where, due to self-heating, the detector remains in a permanent resistive state until the bias current is reduced. Since our $NbSe_2$ detectors have a small normal state resistance (~50 Ω), latching occurs even if a small resistor (25–50 Ω) is placed in parallel with the detector.[39]

At 390 μA, just above I_r, the detector is latched by a strong optical pulse, but is able to recover superconductivity if a low power pulse is used. When the laser is attenuated to ~500 fJ per pulse (Fig. 5), the device is at the boundary between these two behaviors. After each optical pulse, the device intermittently latches or recovers superconductivity with a long decay time >100 ns. For a lower bias current ~220 μA, the 90%–10% decay time is reduced to 2.4 ns. The right axis of Fig. 5 is the voltage normalized to the amplitude of response measured under bright illumination (1100 fJ per pulse), where the entire length is assumed resistive. It therefore shows the approximate length of the resistive region normalized to the full length of the $NbSe_2$ flake, L. In both traces, the length of the resistive region initially settles to 0.44L, where they diverge then. The latching pulse (A) grows to 0.56L and

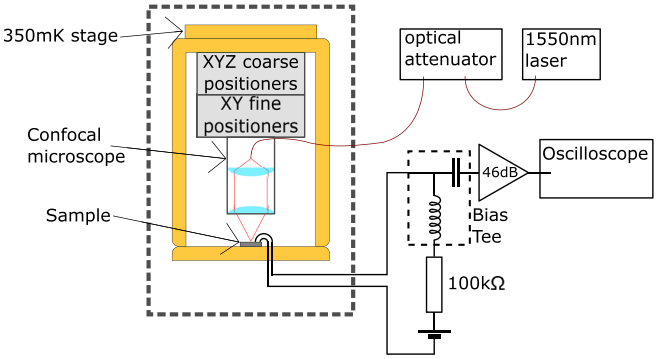

FIG. 4. Experimental setup used to measure the photoresponse. Attenuated laser pulses are focused on a current biased sample using a cryogenic confocal microscope. The resulting voltage pulses are amplified at room temperature before being counted or viewed on an oscilloscope. Since the $NbSe_2$ flakes have a resistance ~ 50 Ω, they are well impedance matched with the transmission line. Thus, the biasing circuit does not include a parallel resistor.

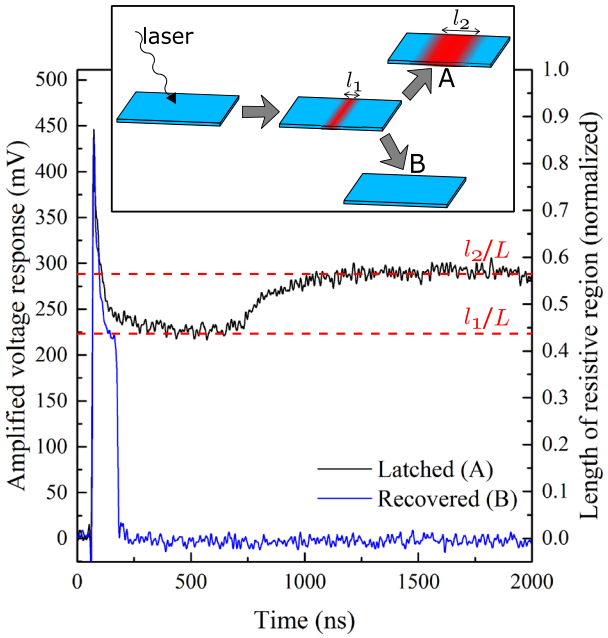

FIG. 5. Oscilloscope traces showing the critical resistive length phenomenon around l_1. The inset illustrates the two possible hotspot evolutions: (a) growth to l_2 and (b) decay to 0 with recovery of superconductivity.

the recovered pulse (B) drops to 0 after further ~20 ns, returning to the superconducting state.

In order to describe the process by which the absorption of radiation causes an electrical response from $NbSe_2$, we consider how an optically stimulated resistive region would evolve within a superconducting flake. This is governed by the balance of Joule heating and heat dissipation.[40,41] Assuming uniform thermal conductivity, heat capacity, and current density ($J = I/A$, where A is the cross-sectional area of the flake), the temperature distribution in the flake will tend toward being one dimensional due to heat diffusion.[42] We model the device as initially at a constant temperature (T_{bath}), in thermal equilibrium with its environment. Current is passed by the Ti/Au electrodes. Their thickness is 55 nm, at least 10 times larger than our $NbSe_2$. We thus assume that the contacts maintain each end of the device at T_{bath}. This geometry was studied analytically in Ref. 40 for the time-independent case, when Joule heating is balanced by thermal dissipation. The current density (J) required to sustain a resistive region of length l, when the materials properties are T-independent, can be written as[40]

$$J^2 = \frac{2\alpha(T_c - T_{bath})\cosh\left(\frac{L}{2}\sqrt{\frac{\alpha}{\kappa d}}\right)}{\rho d\left\{\cosh\left(\frac{L}{2}\sqrt{\frac{\alpha}{\kappa d}}\right) - \cosh\left[\left(\frac{L}{2} - l\right)\sqrt{\frac{\alpha}{\kappa d}}\right]\right\}}, \quad (2)$$

where κ is the T-dependent thermal conductivity of $NbSe_2$,[43] l is the length of the self-sustaining resistive region, ρ is the resistivity of the flake in the normal state, d is the thickness of the superconducting flake, and α is the heat transfer coefficient to the substrate, a sample dependent parameter.

Equation (2) shows that J required to sustain a resistive region of length l reaches a minimum, J_{latch}, when $l = L/2$. Therefore, the bias current must be $> I_{latch} = AJ_{latch}$ for the superconducting flake to have a steady state resistance. Using Eq. (2) to solve for l, we find that any current $> I_{latch}$ has two solutions l_1 and $l_2 = L - l_1$, with l_1 being the smaller of the two lengths. For these, the electrical power dissipated in the resistive region will be balanced by thermal diffusion. However, although both are valid solutions, only l_2 is stable in time. l_1 is unstable, since if $l < l_1$, the resistive region will cool and therefore shrink, whereas, if $l > l_1$, the region will be heated and therefore expand. In either case, the resistive length will be driven away from l_1. In contrast, there will be negative electrothermal feedback around l_2, thus a self-sustaining resistive region will settle to this length. l_1 can therefore be viewed as a critical length. If the hotspot length decays below l_1, the resistive region will not be self-sustaining, and superconductivity will be reestablished (Fig. 5 pulse B). If the hotspot length remains above l_1, it will eventually grow to l_2. This results in a latched resistive state, with the steady state resistance of the device proportional to l_2 (Fig. 5 pulse A).

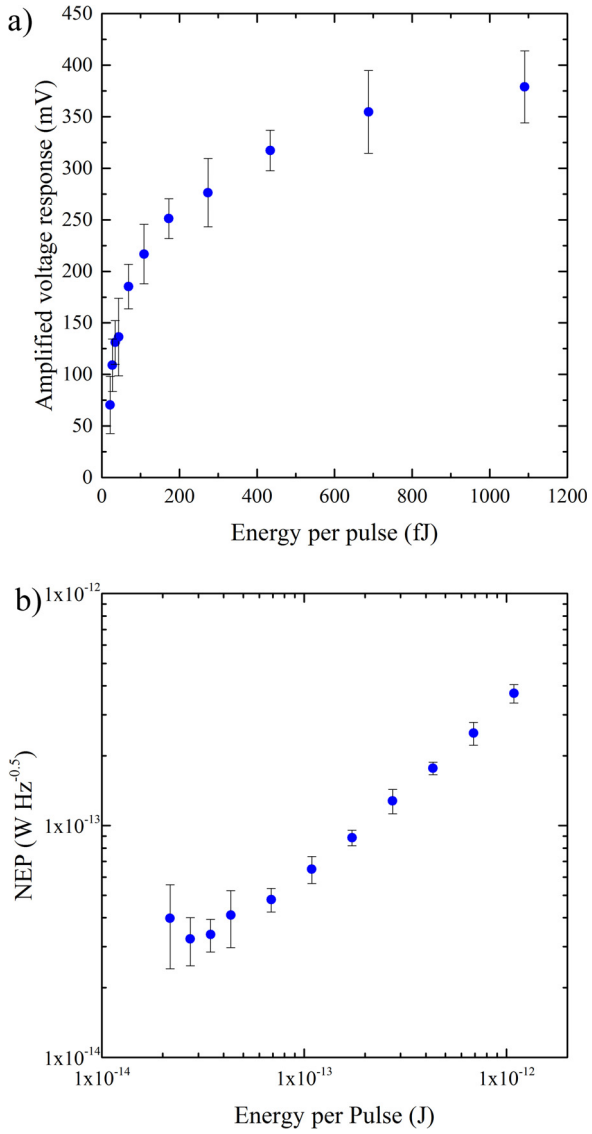

FIG. 6. (a) Amplitude of voltage transients under pulsed illumination with varying laser pulse energy for 230 μA bias current at 5 K. (b) NEP as a function of laser energy, calculated by dividing the spectral noise density by the responsivity.

To demonstrate the energy dependent nature of the photoresponse, the $NbSe_2$ flake in Fig. 3 is biased at 230 μA (0.91I_c) at 5 K and illuminated with single shot laser pulses of energy ranging from 20 to 1100 fJ, Fig. 6(a). The amplitude of the voltage response increases with laser energy and starts saturating ~500 fJ. This behavior can be understood as the laser driving a section of the flake into the resistive state. As the laser energy increases, so does the size of the resistive region. This occurs until the resistive region approaches the total length of the flake, causing saturation of the voltage response. The responsivity of the detector (161 V W^{-1} at 27 fJ per pulse) is calculated by dividing the amplitude of measured voltage transients [Fig. 6(a)] by the maximum instantaneous power of the laser pulses and by the amplifier gain (46 dB). As shown in Fig. 6(b), the NEP of the detector reaches a minimum ~32 fW Hz$^{-0.5}$ at 5 K. This is calculated by dividing the noise spectral density of the detector (5.21×10^{-12} V Hz$^{-0.5}$) by its responsivity.[20] Since the maximum instantaneous power of the laser is used to calculate responsivity, this NEP is an upper bound. For comparison, infrared graphene hot electron bolometers were reported with an electrical NEP ~32 fW Hz$^{-0.5}$ at 5 K (Ref. 18) and commercial InGaAs photodiodes have an NEP range ~5–1000 fW Hz$^{-0.5}$ (Refs. 19 and 20).

13 superconducting $NbSe_2$ detectors were tested, all yielding similar photoresponses. The detectors survive at least 3 thermal cycles. After storage in vacuum for 3 months, ~5% reduction in I_c is observed, assigned to $NbSe_2$ oxidation.

In summary, we prepared hBN encapsulated $NbSe_2$ flakes 2–10 layers thick. These are superconducting and photosensitive at 1550 nm, with an energy dependent response when illuminated. The optical NEP of the detectors is as low as 32 fW Hz$^{-0.5}$ at 5 K, competitive with graphene based hot electron bolometers and commercial photodiodes. The optical absorption could be further improved by integration with optical cavities, waveguides, or plasmonic structures.

We thank L. Baker, D. Morozov, R. Health, R. Kirkwood, and A. Lombardo for useful discussions. We acknowledge funding from ERC Grant Nos. IRIS 649604 and Hetero2D; EPSRC Grant Nos. EP/K01711X/1, EP/K017144/1, EP/N010345/1, and EP/L016087/1; the EU Graphene and Quantum Flagships; the Royal Society and EPSRC International Network Grant No. EP/P026311/1 and Programme Grant No. EP/N0172421/1; and from the Elemental Strategy Initiative by MEXT, Japan and CREST (JPMJCR15F3), JST.

REFERENCES

[1]P. L. Richards, J. Appl. Phys. **76**, 1 (1994).
[2]A. M. Kadin, M. Leung, and A. D. Smith, Phys. Rev. Lett. **65**, 25 (1990).
[3]K. D. Irwin, G. C. Hilton, D. A. Wollman, and J. M. Martinis, Appl. Phys. Lett. **69**, 13 (1996).
[4]J. J. A. Baselmans, J. Low Temp. Phys. **167**, 292 (2012).
[5]G. N. Gol'tsman, O. Okunev, G. Chulkova, A. Lipatov, A. Semenov, K. Smirnov, B. Voronov, A. Dzardanov, C. Williams, and R. Sobolewski, Appl. Phys. Lett. **79**, 705 (2001).

[6]C. M. Natarajan, M. G. Tanner, and R. H. Hadfield, Supercond. Sci. Technol. **25**, 063001 (2012).
[7]F. Marsili, V. B. Verma, J. A. Stern, S. Harrington, A. E. Lita, T. Gerrits, I. Vayshenker, B. Baek, M. D. Shaw, R. P. Mirin, and S. W. Nam, Nat. Photonics **7**, 210 (2013).
[8]R. H. Hadfield, Nat. Photonics **3**, 696 (2009).
[9]H. Takesue, S. W. Nam, Q. Zhang, R. H. Hadfield, T. Honjo, K. Tamaki, and Y. Yamamoto, Nat. Photonics **1**, 343 (2007).
[10]A. McCarthy, N. J. Krichel, N. R. Gemmell, X. Ren, M. G. Tanner, S. N. Dorenbos, V. Zwiller, R. H. Hadfield, and G. S. Buller, Opt. Express **21**, 8904 (2013).
[11]A. Engel, J. Renema, K. Il'in, and A. Semenov, Supercond. Sci. Technol. **28**, 114003 (2015).
[12]A. Semenov, A. Engel, H.-W. Hübers, K. Ilin, and M. Siegel, Eur. Phys. J. B **47**, 495 (2005).
[13]R. Lusche, A. Semenov, K. Ilin, M. Siegel, Y. Korneeva, A. Trifonov, A. Korneev, G. Goltsman, D. Vodolazov, and H. W. Hbers, J. Appl. Phys. **116**, 043906 (2014).
[14]Y. Korneeva, D. Y. Vodolazov, A. V. Semenov, I. Florya, N. Simonov, E. Baeva, A. A. Korneev, G. N. Goltsman, and T. M. Klapwijk, Phys. Rev. Appl. **9**, 064037 (2018).
[15]E. Revolinsky, G. A. Spiering, and D. J. Beerntsen, J. Phys. Chem. Solids **26**, 1029 (1965).
[16]R. F. Frindt, Phys. Rev. Lett. **28**, 299 (1972).
[17]Y. Cao, A. Mishchenko, G. L. Yu, E. Khestanova, A. P. Rooney, E. Prestat, A. V. Kretinin, P. Blake, M. B. Shalom, C. Woods *et al.*, Nano Lett. **15**, 4914 (2015).
[18]J. Yan, M.-H. Kim, J. A. Elle, A. B. Sushkov, G. S. Jenkins, H. M. Milchberg, M. S. Fuhrer, and H. D. Drew, Nat. Nanotechnol. **7**, 472 (2012).
[19]See https://www.thorlabs.com/ for commercially available InGaAs photodiodes.
[20]S. Donati, *Photodetectors: Devices, Circuits and Applications* (Prentice Hall, 2000).
[21]C. Casiraghi, A. Hartschuh, E. Lidorikis, H. Qian, H. Harutyunyan, T. Gokus, K. S. Novoselov, and A. C. Ferrari, Nano Lett. **7**, 2711 (2007).
[22]M. M. Benameur, B. Radisavljevic, J. S. Heron, S. Sahoo, H. Berger, and A. Kis, Nanotechnology **22**, 125706 (2011).
[23]See http://www.hqgraphene.com/ for a source of high quality 2D crystals.
[24]M. S. El-Bana, D. Wolverson, S. Russo, G. Balakrishnan, D. M. Paul, and S. J. Bending, Supercond. Sci. Technol. **26**, 125020 (2013).
[25]T. Taniguchi and K. Watanabe, J. Cryst. Growth **303**, 525 (2007).
[26]K. S. Novoselov, D. Jiang, F. Schedin, T. J. Booth, V. V. Khotkevich, S. V. Morozov, and A. K. Geim, Proc. Natl. Acad. Sci. U. S. A. **102**, 10451 (2005).
[27]A. Castellanos-Gomez, M. Buscema, R. Molenaar, V. Singh, L. Janssen, H. S. J. van der Zant, and G. A. Steele, 2D Mater. **1**, 011002 (2014).
[28]C. Palacios-Berraquero, M. Barbone, D. M. Kara, X. Chen, I. Goykhman, D. Yoon, A. K. Ott, J. Beitner, K. Watanabe, T. Taniguchi, A. C. Ferrari, and M. Atatre, Nat. Commun. **7**, 12978 (2016).
[29]D. G. Purdie, N. M. Pugno, T. Taniguchi, K. Watanabe, A. C. Ferrari, and A. Lombardo, Nat. Commun. **9**, 5387 (2018).
[30]A. C. Ferrari and D. M. Basko, Nat. Nanotechnol. **8**, 235 (2013).
[31]X. Zhang, W. P. Han, J. B. Wu, S. Milana, Y. Lu, Q. Q. Li, A. C. Ferrari, and P. H. Tan, Phys. Rev. B **87**, 115413 (2013).
[32]P. H. Tan, W. P. Han, W. J. Zhao, Z. H. Wu, K. Chang, H. Wang, Y. F. Wang, N. Bonini, N. Marzari, N. Pugno *et al.*, Nat. Mater. **11**, 294 (2012).
[33]S. Reich, A. C. Ferrari, R. Arenal, A. Loiseau, I. Bello, and J. Robertson, Phys. Rev. B **71**, 205201 (2005).
[34]R. Arenal, A. C. Ferrari, S. Reich, L. Wirtz, J.-Y. Mevellec, S. Lefrant, A. Rubio, and A. Loiseau, Nano Lett. **6**, 1812 (2006).
[35]R. J. Nemanich, S. A. Solin, and R. M. Martin, Phys. Rev. B **23**, 6348 (1981).
[36]J. Li, R. A. Kirkwood, L. J. Baker, D. Bosworth, K. Erotokritou, A. Banerjee, R. M. Heath, C. M. Natarajan, Z. H. Barber, M. Sorel, and R. H. Hadfield, Opt. Express **24**, 13931 (2016).
[37]M. Tinkham, *Introduction to Superconductivity*, 2nd ed. (Dover Publications, 2004).
[38]A. N. Zotova and D. Y. Vodolazov, Supercond. Sci. Technol. **26**, 075008 (2013).
[39]A. J. Annunziata, D. F. Santavicca, L. Frunzio, G. Catelani, M. J. Rooks, A. Frydman, and D. E. Prober, J. Appl. Phys. **108**, 084507 (2010).
[40]W. J. Skocpol, M. R. Beasley, and M. Tinkham, J. Appl. Phys. **45**, 4054 (1974).
[41]A. Blois, S. Rozhko, L. Hao, J. C. Gallop, and E. J. Romans, Supercond. Sci. Technol. **30**, 014003 (2017).
[42]A. N. Zotova and D. Y. Vodolazov, Phys. Rev. B **85**, 024509 (2012).
[43]E. Boaknin, M. A. Tanatar, J. Paglione, D. Hawthorn, F. Ronning, R. W. Hill, M. Sutherland, L. Taillefer, J. Sonier, S. M. Hayden, and J. W. Brill, Phys. Rev. Lett. **90**, 117003 (2003).